Scripta Materialia 173 (2019) 46–50

Contents lists available at ScienceDirect

Scripta Materialia

journal homepage: www.elsevier.com/locate/scriptamat

Competition for impurity atoms between defects and solid solution during high pressure torsion

A.A. Mazilkin [a,c], B.B. Straumal [a,b,c,d,*], A.R. Kilmametov [c], T. Boll [e,f], B. Baretzky [c], O.A. Kogtenkova [a], A. Korneva [g], P. Zięba [g]

[a] Institute of Solid State Physics, Russian Academy of Sciences, Ac. Ossipyan str. 2, Chernogolovka 142432, Russia
[b] Scientific Center in Chernogolovka, Russian Academy of Sciences, Lesnaya str. 9, Chernogolovka 142432, Russia
[c] Institute for Nanotechnology, Karlsruhe Institute of Technology (KIT), Hermann-von-Helmholtz-Platz 1, 76344 Eggenstein-Leopoldshafen, Germany
[d] National University of Science and Technology "MISIS", Leninskii prosp. 4, 119049 Moscow, Russia
[e] Institute for Applied Materials (IAM-WK), Karlsruhe Institute of Technology (KIT), Hermann-von-Helmholtz-Platz 1, 76344 Eggenstein-Leopoldshafen, Germany
[f] Karlsruhe Nano Micro Facility (KNMF), Karlsruhe Institute of Technology (KIT), Hermann-von-Helmholtz-Platz 1, 76344 Eggenstein-Leopoldshafen, Germany
[g] Institute of Metallurgy and Materials Science, Polish Academy of Sciences, Reymonta St. 25, 30-059 Cracow, Poland

ARTICLE INFO

Article history:
Received 27 May 2019
Received in revised form 30 July 2019
Accepted 1 August 2019
Available online xxxx

Keywords:
Nano-crystalline metals
Grain boundaries
Segregation
Cu-based alloys
High-pressure torsion

ABSTRACT

During high-pressure torsion (HPT) the dynamic equilibrium establishes with a certain steady-state composition of the solid solution along with the grain refinement by a factor of more than thousand. The formation of such HPT steady-state in copper alloys with Co, Ag and In has been studied. If precipitates of a second phase were present in the sample before HPT, their dissolution led to the enrichment in the (Cu) matrix solid solution. If precipitates of a second phase were absent, the HPT led to the depletion in the (Cu) matrix due to the segregation in newly formed defects like grain boundaries.

Recently we observed that two processes compete with each other during high pressure torsion (HPT) of Cu-based binary alloys: (1) decomposition (depletion) of solid solution with formation of precipitates and (2) dissolution of precipitates with enrichment of solid solution [1,2]. As a result, a dynamic equilibrium is reached and a steady state is formed after about two HPT anvil rotations. A certain steady state concentration c_{ss} of second component was established in the solid solution. If the concentration c_s in the solid solution before HPT is lower than c_{ss}, HPT leads to the partial dissolution of precipitates, and c_s increases up to c_{ss}. If $c_s > c_{ss}$ the solid solution decomposes partially, and c_s decreases down to c_{ss}. What happens if the total concentration of the second component is $c_{tot} < c_{ss}$?

HPT always leads to the strong grain refinement and formation of other defects like vacancies, dislocations and grain boundary (GB) triple junctions (GBTJs) [3]. In case of Cu-based alloys, the grain size typically decreases by about the factor of 1000 [1,2,4–6]. The second component usually form segregation layers in GBs and line complexions (segregation tubes) in dislocations and GBTJs. These segregation layers and tubes newly formed during HPT can "consume" the atoms of the second component both from solid solution and precipitates. In case of GBs it can be (a) monolayer Gibbs segregation, (b) multilayer Fowler-Guggenheim segregation [7] or (c) few nanometer thin layers of GB phases [8–11]. For example, GBs and other defects in nanograined oxides can hide tens of percent of second component atoms [12]. In this case we have to consider the competition between three "refugia" for alloying atoms (Fig. 1): solid solution, precipitates, and defects (like dislocations, GBs and GBTJs). This is true if $c_{tot} > c_{ss}$. If $c_{tot} < c_{ss}$, the precipitates are absent, and only the competition between solid solution and defects segregation layers and tubes takes place (Fig. 1). If the defects segregation is high enough, the alloying atoms would leave the solid solution, and c_s would decrease during HPT in comparison with the concentration before HPT. The experimental search for such a depletion effect in Cu—Ag, Cu—Co and Cu—In alloys is the goal of this work [1,2,13]. The published data witness strong segregation of silver in (Cu)/(Cu) GBs [14–17].

The following copper alloys have been prepared from the high-purity components (5 N5 Cu, 4 N8 Ag, 4 N4 Co and 5 N4 In) by vacuum induction melting: Cu with 2.6 and 5.3% Co; 2.4 and 4.9 Ag; 2.3 and 5.8% In (in at. %). For the HPT processing, the 0.6 mm thick disks sealed into evacuated silica ampoules with a residual pressure of approximately 4×10^{-4} Pa and then annealed: Cu—Co at 570 °C for 450 h and 900 °C for 67 h; Cu—Ag at 600 °C for 770 h and at 800 °C for 290 h; Cu—In at

* Corresponding author at: Institute of Solid State Physics, Russian Academy of Sciences, Chernogolovka, Moscow District 142432, Russia.
E-mail address: straumal@issp.ac.ru (B.B. Straumal).

https://doi.org/10.1016/j.scriptamat.2019.08.001
1359-6462/

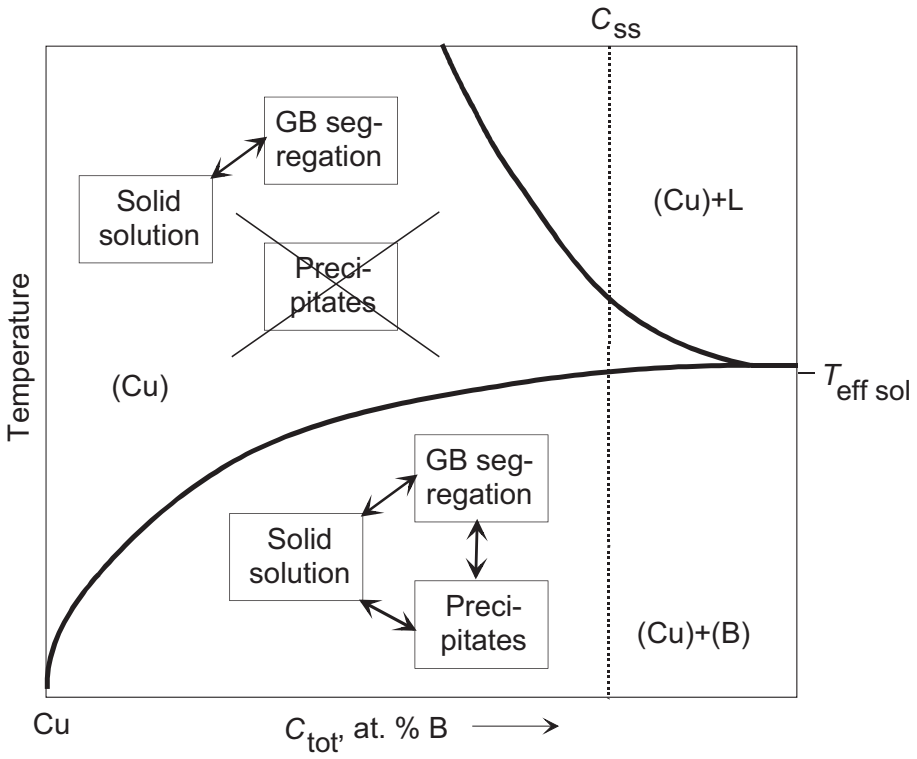

Fig. 1. Scheme of the binary phase diagram for the Cu-based alloy showing the steady-state concentration in the HPT dynamic equilibrium c_{ss}, the effective temperature for the composition of matrix solid solution T_{eff}^{sol}, and the competition between three "refugia" for alloying atoms: solid solution, precipitates and defects. Only GBs are shown for simplicity.

570 °C for 400 h. The succeeding HPT took place at room temperature and 6 GPa for 5 rotations at 1 rpm in a custom built computer controlled HPT device (W. Klement GmbH, Lang, Austria). The samples for the microstructure studies were cut from the HPT-processed disks at a distance of 3 mm from the sample center. The transmission electron microscopy (TEM) is performed in a TECNAI G2 FEG super TWIN at 200 kV. TEM thin foils were prepared by a twin-jet polishing technique using D2 Struers electrolyte. The X-ray diffraction (XRD) patterns were obtained using Bragg–Brentano geometry in a powder diffractometer (Philips X'Pert) with Cu-Kα radiation. For atom probe tomography (APT) samples were prepared with a dual beam Zeiss Auriga with the standard lift-out method on a microtip coupon [18]. These samples were measured with a LEAP (Local electrode atom probe) 4000× HR at temperatures of 25 K to 50 K with laser energy was 30–100 pJ per pulse at a frequency of 100 kHz. For the evaluation of the APT results the IVAS 3.6.14 software from Ametek was used.

Fig. 2 shows the XRD patterns for the alloys before and after the HPT deformation. The Cu–5.3% Co alloy (Fig. 2a) was annealed before HPT at 570 °C, i.e. below solvus line in the (Cu) + (Co) two-phase area of the Cu—Co phase diagram [19]. The respective XRD pattern contains peaks of the (Cu) solid solution and weak peaks of the (Co) precipitates. The annealing temperature for the Cu–2.6% Co alloy before HPT was at 900 °C, i.e. in one-phase (Cu) area of Cu—Co phase diagram. Respectively, the XRD pattern showed only peaks of (Cu) solid solution and no cobalt peaks, which indicates the presence of only the (Cu) phase.

In Fig. 2b the XRD patterns are shown for the Cu–2.4% Ag and Cu–4.9% Ag alloys. The Cu–4.9% Ag alloy was annealed before HPT at 600 °C, i.e. below the solvus line in the (Cu) + (Ag) two-phase area of the Cu—Ag phase diagram [19], which is confirmed by the XRD pattern containing the peaks of the (Cu) solid solution and weak peaks of the (Ag) precipitates. The XRD pattern of the Cu–2.4% Ag alloy annealed before HPT at 800 °C (one-phase area) contains only the peaks of the (Cu) solid solution and no silver peaks.

Both Cu—In alloys were annealed before HPT at 570 °C in the (Cu) one-phase area of the Cu—In phase diagram [19] and contain only peaks of (Cu) solid solution and no peaks of Cu—In intermetallic phases in the XRD patterns (Fig. 2c).

HPT led to strong grain refinement in all investigated alloys. The grain size decreased from ~500 μm to ~150 nm. Fig. 3 shows an example of the microstructure for Cu – 5.3% Co alloy after HPT. As a result, the peaks in respective XRD patterns broadened in comparison to those before HPT. In the Cu–5.3% Co alloy the (Co) peaks almost disappeared after HPT and the XRD peaks of copper shifted to the right (shown with arrows in Fig. 2a). This means that Co precipitates were also fragmented and almost dissolved, and c_s increased. It is because the addition of Co into the Cu lattice decreases the lattice parameter. In the Cu–2.6% Co alloy, (Cu) peaks moved to the left after HPT, in the direction of pure copper, which implies that the Cu-matrix is "purified" and Co atoms disappeared from Cu-based solid solution.

In the Cu– 4.9% Ag alloy the (Ag) peaks almost disappeared after HPT, and Cu peaks shifted to the left, as shown in Fig. 2b. Thus, Ag precipitates were fragmented, almost dissolved and c_s decreased. It is because silver addition increases the lattice parameter in copper. More exact experiments demonstrated recently that the Ag precipitates were not only fragmented [20] and the content of silver in copper-matrix increased up to c_{ss}, but also the concentration of copper in silver precipitates increased towards a steady state one [21]. In the Cu–2.4% Ag alloy, (Cu) peaks moved to the right after HPT, in the direction of pure copper. As a result, the Cu-matrix after the deformation contains less silver than in the initial state.

For both Cu—In alloys the XRD profiles show no measurable difference in the position of (Cu) peaks before and after HPT (Fig. 2c).

APT reveals that indeed there is segregation in GBs and other defects for both, pre- and after HPT samples of Cu–2.4% Ag alloy. Fig. 4a shows a heat map of a selected slice, representing the Ag-ion density. Low Ag-ion density is blue, high Ag-ion density is greenish. The silver density

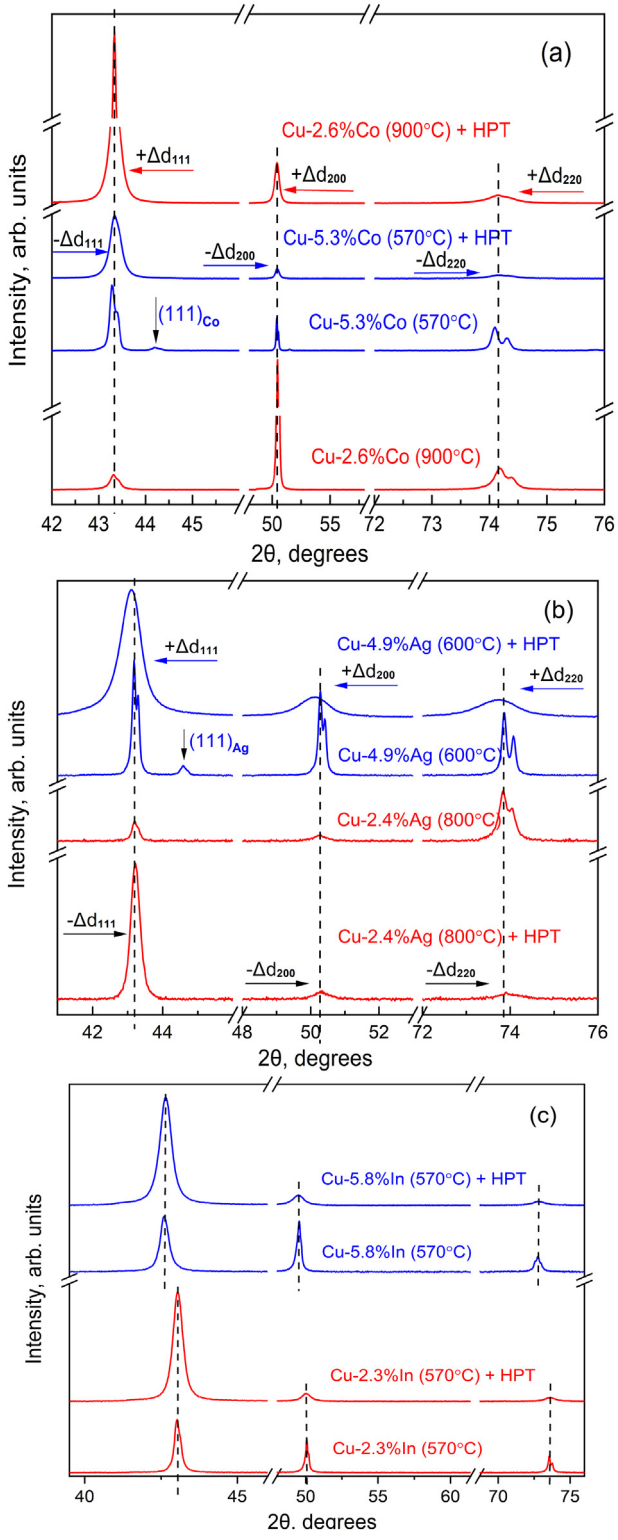

Fig. 2. X-ray diffraction patterns of (a) Cu—Co, (b) Cu—Ag and (c) Cu—In alloys before and after HPT. The patterns are vertically shifted for better comparison.

interval is between 0 and 3 atoms/nm^3, the curved slope of a high density indicates a GB (marked by arrows). The possibility to rotate the three-dimensional APT image permitted to find the two-dimensional curved "tape" enriched by silver atoms. It corresponds to the Ag segregation in a (Cu)/(Cu) GB. Other Ag-enriched areas are point-like or linear. They correspond to other defects like dislocations. The radial distribution function [22] around Ag atoms is shown in Fig. 4b. An Ag

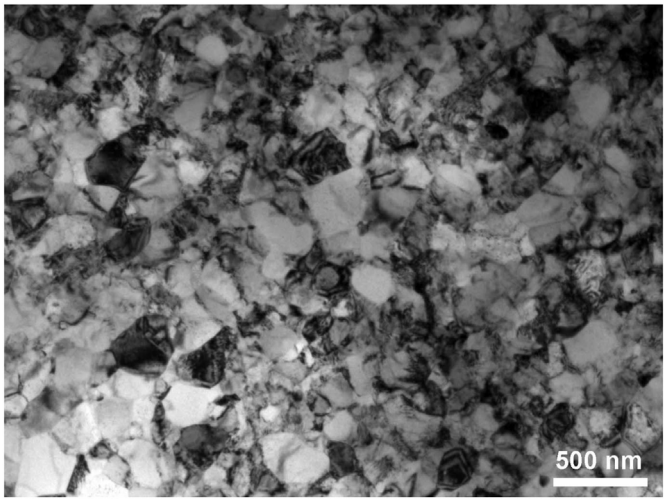

Fig. 3. Bright field TEM micrograph of annealed Cu – 5.3% Co, 570 °C alloy after HPT.

segregation is revealed by the increased normalized Ag concentration close to the centers of Ag atoms. The Ag segregation slightly increased in the samples subjected to HPT in comparison with ones before HPT. It means that after HPT more silver atoms are surrounded by other silver atoms than before HPT. From the Fig. 4b, it is possible also to estimate the width of the segregation layer, which is around 1 nm thick. Since the overall segregation effect is rather small, one has to consider the possibility that the observed segregation could be an effect of preferential evaporation at the GBs. The expected evaporation fields of Ag with 24 V/nm and Cu with 30 V/nm [23] differ enough to make this possible. Thus we changed the evaporation conditions by decreasing the temperature from 50 to 25 K. The observed segregation effect was retained, suggesting that the segregation is true.

We observed that if the initial alloy contained Co or Ag precipitates, HPT led to their dissolution, and Co or Ag concentration in the solid solution increased towards c_{ss} like in [1,2]. It is because $c_s < c_{ss}$ in the studied alloys. If the samples contained only solid solution without precipitates, the Co or Ag concentration in the solid solution decreased. After HPT the grain size decreased more than thousand times and a lot of new GBs as well as dislocations and GBTJs formed together with the respective segregation layers and tubes. If the alloy contained precipitates, they were used as the sources for defects segregation layers and tubes. If precipitates were absent before HPT, the solid solution served instead as the source to form the segregation. If GB and GBTJ segregation is strong enough (like in Cu—Co and Cu—Ag alloys), the latter process led to the depletion of a solid solution. In case of weak segregation (like in Cu—In alloys) the depletion of the solid solution was not measurable.

From the obtained data one can estimate the impurity concentration in the GB segregation layers. Let us suppose for the estimation that all impurity segregates in GBs and GBTJs. GBTJs can be considered as superposition of GB segregation layers [24]. The lattice period of (Cu) in Cu–2.6% Co alloy before HPT was $a = 0.36137$ nm and after HPT it was $a = 0.36147$ nm. This means that, according to the Vegard law the (Cu) solid solution contained 2.6% Co before HPT, and only about 1.2% Co after HPT [1]. Thus, about 1.4% Co was used for the formation of GB segregation. Let us suppose that the Cu grains have the shape of tetrakaidecahedron [25] which gives the least GB surface. For GB thickness $\delta = 1$ nm and for the grain size of 100 nm, the GB layers occupy about 1.65% of the total volume. In this case Co atoms would occupy about 85% of the sites in GB layers. The GB segregation factor $s = 71$ is the ratio between GB and bulk concentration. Similarly, the lattice period of (Cu) in Cu–2.4% Ag sample before HPT was $a = 0.362728$ nm, and after HPT $a = 0.362539$ nm, i.e. the (Cu) solid solution lost about 0.3% Ag [2,26–28]. If the grain size was 100 nm silver atoms would

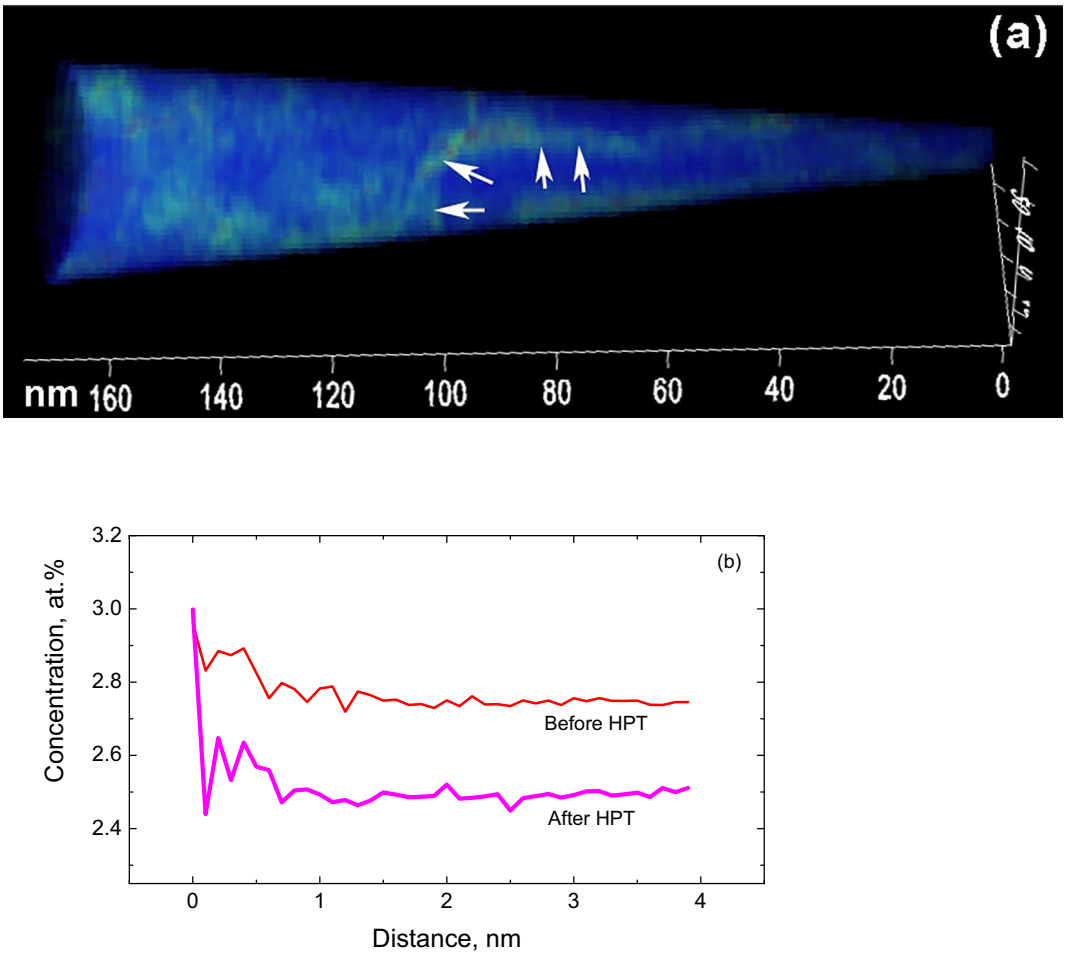

Fig. 4. APT of Cu – 2.4% Ag sample after HPT (a) Ag heatmap, concentration interval is between 0 and 3 atoms/nm^3 Ag, scale in nm, (b) radial distribution function of samples before and after HPT.

occupy about 20% of the GB sites. $s = 10$ for the Cu–2.4% Ag alloy. In the Cu–2.3% In alloy the change of lattice period before and after HPT does not exceed $\Delta a = 0.00005$ nm. In Cu—In alloys this corresponds to about 0.2% In [3,29–32]. For the grain size of 100 nm it means that the In enrichment at GBs is below 2% and s ~1. Thus, the observed GB segregation decreases in the sequence Co → Ag → In.

In Table 1 the values of s and segregation enthalpy H_s measured by radiotracer method and Auger electron spectroscopy are given. The extrapolation of s for Cu—Ag and Cu—Co systems for the temperature of a HPT treatment at 25 °C gives $s > 10^3$–10^4. The estimated values of $s = 71$ for the Cu–2.6% Co and $s = 10$ for Cu– 2.4% Ag after HPT correlate with the radiotracer data of s at high temperature of $T > 500$ °C. Thus, the GB enrichment after HPT at $T = 25$ °C is similar to that after conventional annealing at a certain effective temperature $T_{eff}^{segr} > 500$ °C. Previously we observed that the composition of the matrix solid solution after HPT in the Cu—Co and Cu—Ag alloys as well as the rate of mass transfer is the same as for conventional annealing at 900 and 700 °C, respectively.

Table 1
GB segregation factor s and segregation enthalpy H_s measured by radiotracer method and Auger electron spectroscopy.

Alloy	s	H_s, kJ/mol	T, °C	Ref.
Co in Cu	10^3	34.7	260–650	[16,33-38]
Ag in Cu	10		150–200	[39,40]
Ag in Cu	10^2–10^3		150–300	[41,42]
Ag in Cu–0.2% Ag	1–4	25	350–600	[43]
Ag in Σ5 (310) [001] symmetric tilt GB	$5\cdot10^2$–$2\cdot10^3$	27–28	260–650	[17,44]

The APT map in Fig. 4a indicates the Ag segregation in (Cu)/(Cu) GBs [42–45]. The two-dimensional "tape" of a (Cu)/(Cu) GB is enriched by silver atoms. The inhomogeneity of silver distribution inside the copper grains reveals segregation in low-angle GBs or dislocations [45]. The radial distribution in Fig. 4b demonstrates that the difference in GB concentration between GBs before and after HPT is not very big, which suggests that the structure of GBs in the steady-state reached after 5 anvil rotations is very close to that after long annealing and, therefore, to the equilibrium one. It is in contradiction to the generally accepted ideas about the formation of non-equilibrium GBs during HPT [46,47]. The radial distribution (Fig. 4b) shows that, indeed, in agreement with the XRD data (Fig. 2b) the silver concentration in the bulk after HPT (~2.5% Ag) is lower than before HPT (~2.75% Ag). We can conclude that the formation of GB segregation layers in GBs newly formed during HPT "consumes" indeed the Ag atoms from the solid solution. Theoretical works also predict the strong Ag segregation in Cu GBs including transition from monolayer to multilayer segregation or even to the thick premelting GB layer [48–59].

It is important to underline that the steady-state establishes during HPT very quickly, after 1–2 anvil rotations, i.e. within 1–2 min at the room temperature [4,60]. The respective mass transfer needed for the redistribution of impurities is equivalent to that performed by the

conventional bulk diffusion at the increased temperature T_{eff}^{diff} [1,2]. The composition of matrix solid solution in the steady-state is also equivalent to the solubility at certain T_{eff}^{sol} [60,61]. In this work we estimated another value, namely T_{eff}^{segr}, based on the GB segregation. All three values are comparable $T_{eff}^{diff} \sim T_{eff}^{sol} \sim T_{eff}^{segr}$. In other words, the state of dynamic equilibrium between defects production and defects relaxation during HPT is indeed similar to the state at a certain increased temperature T_{eff}.

To conclude, HPT leads to the redistribution of a second component between the bulk solid solution, the precipitates of a second phase and the grain boundary segregation layers. In case the precipitates in the alloy are absent, the segregation is formed on the newly appeared GBs at the expense of the depletion of the matrix solid solution. Based on this effect, we concluded that the GB segregation decreases in the sequence Co → Ag → In.

Thus, the goal of this short work was to demonstrate the principle possibility to observe and quantitative measure the GB adsorption by comparing the position of XRD peaks before and after HPT in coarse-grained and fine-grained samples. We demonstrated that it is possible and the effect is measurable in Cu—Ag and Cu—Co alloys. It is possible when the alloys are annealed in such a way that precipitates of a second phase are absent and “new” grain boundaries “soak” silver (or cobalt) from solid solution leading to its impoverishment. In turn, it shifts the XRD peaks. Respective GB adsorption is also visualized by APT. Using this approach it will be possible to compare the GB adsorption in alloys with different alloy concentration and after different heat treatments, as well as after HPT in different conditions (like temperature, pressure or strain rate) with a hope to find the transitions from single- to multilayer GB adsorption like in other alloys [7,62–64].

Acknowledgements

The authors thank Delphine Chassaing for the preparation of APT samples. This work was partially supported by Ministry of Education and Science of the Russian Federation in the framework of the Program to Increase the Competitiveness of NUST “MISiS”, the National Science Centre of Poland (grant OPUS 2014/13/B/ST8/04247), by the Russian Foundation for Basic Research (grant 18-03-00067). The part of research has been performed within the Accredited Testing Laboratories with certificate No. AB 120 issued by the Polish Centre of Accreditation according to European standard PN-ISO/IEC 17025:2005 and EA-2/15.

References

[1] B.B. Straumal, A.R. Kilmametov, Yu. Ivanisenko, L. Kurmanaeva, B. Baretzky, Yu.O. Kucheev, P. Zięba, A. Korneva, D.A. Molodov, Mater. Lett. 118 (2014) 111.
[2] B.B. Straumal, V. Pontikis, A.R. Kilmametov, A.A. Mazilkin, S.V. Dobatkin, B. Baretzky, Acta Mater. 122 (2017) 60.
[3] B. Straumal, R. Valiev, O. Kogtenkova, P. Zieba, T. Czeppe, E. Bielanska, M. Faryna, Acta Mater. 56 (2008) 6123.
[4] B.B. Straumal, A.R. Kilmametov, A. Korneva, A.A. Mazilkin, P.B. Straumal, P. Zięba, B. Baretzky, J. Alloys Comp. 707 (2017) 20.
[5] N. Lugo, N. Llorca, J.M. Cabrera, Z. Horita, Mater. Sci. Eng. A 477 (2008) 366.
[6] J. Čížek, M. Janeček, O. Srba, R. Kuzel, Z. Barnovska, I. Prochazka, S. Dobatkin, Acta Mater. 59 (2011) 2322.
[7] L.-S. Chang, E. Rabkin, B.B. Straumal, S. Hoffmann, B. Baretzky, W. Gust, Defect Diff, Forum 156 (1998) 135.
[8] E.I. Rabkin, L.S. Shvindlerman, B.B. Straumal, Int. J. Mod. Phys. B 5 (1991) 2989.
[9] A. Subramaniam, C. Koch, R.M. Cannon, M. Rühle, Mater. Sci. Eng. A 422 (2006) 3.
[10] W.D. Kaplan, D. Chatain, P. Wynblatt, W.C. Carter, J. Mater. Sci. 48 (2013) 5681.
[11] P.R. Cantwell, M. Tang, S.J. Dillon, J. Luo, G.S. Rohrer, M.P. Harmer, Acta Mater. 62 (2014) 1.
[12] B.B. Straumal, B. Baretzky, A.A. Mazilkin, S.G. Protasova, A.A. Myatiev, P.B. Straumal, J. Eur. Ceram. Soc. 29 (2009) 1963.
[13] B.B. Straumal, A.R. Kilmametov, A.A. Mazilkin, L. Kurmanaeva, Y. Ivanisenko, A. Korneva, P. Zięba, B. Baretzky, Mater. Letters 138 (2015) 255.
[14] J. Hickman, Y. Mishin, Phys. Rev. B 93 (2016) 224108.
[15] F. Berthier, J. Creuze, R. Tetot, B. Legrand, Phys. Rev. B 65 (2002) 195413.
[16] D. Gaertner, G. Wilde, S.V. Divinski, Acta Mater. 127 (2017) 407.
[17] S.V. Divinski, H. Edelhoff, S. Prokofjev, Phys. Rev. B 85 (2012) 144104.
[18] D.J. Larson, T.J. Prosa, R.M. Ulfig, B.P. Geiser, T.F. Kelly, Local Electrode Atom Probe Tomography, Springer, Berlin etc., 2013
[19] T.B. Massalski (Ed.), Binary Alloy Phase Diagrams, ASM International, Metals Park, Ohio, USA, 1990.
[20] A. Korneva, B. Straumal, A. Kilmametov, R. Chulist, G. Cios, B. Baretzky, P. Zięba, Materials 12 (2019) 447.
[21] B.B. Straumal, A.R. Kilmametov, O.A. Kogtenkova, A.A. Mazilkin, B. Baretzky, A. Korneva, P. Zięba, Int. J. Mater. Res. 110 (2019).
[22] A. Heinrich, T. Al-Kassab, R. Kirchheim, Mater. Sci. Eng. A 353 (2003) 92.
[23] M.K. Miller, A. Cerezo, M.G. Hetherington, G.D.W. Smith, Atom Probe Field Ion Microscopy, Oxford Science Publications, Oxford, 1996.
[24] B.B. Straumal, O. Kogtenkova, P. Zięba, Acta Mater. 56 (2008) 925.
[25] W.F. Hosford, Materials Science: An Intermediate Text, Cambridge University Press, Cambridge, UK, 2007.
[26] E. Schmid, G. Siebel, Z. Phys. 85 (1932) 36.
[27] N. Ageew, M. Hansen, G. Sachs, Z. Phys. 66 (1930) 350.
[28] H.D. Megaw, Phil. Mag. 14 (1932) 130.
[29] E.A. Owen, J. Rogers, J. Inst. Met. 57 (1935) 257.
[30] F. Weibke, H. Eggers, Zt. Anorgan. Allgem. Chem. 220 (1934) 273.
[31] E.A. Owen, E.A.O. Roberts, J. Inst. Met. 81 (1953) 479.
[32] R.O. Jones, E.A. Owen, J. Inst. Met. 83 (1954) 445.
[33] P.H. Stirling, G.V. Raynor, J. Inst. Met. 84 (1956) 519.
[34] H. Mehrer (Ed.), Diffusion in Solid Metals and Alloys, Landolt-Börnstein New Series, Gr III, vol. 26, Springer-Verlag, Berlin, 1990.
[35] P. Lejček, Springer Series in Materas Science, vol. 136, Springer-Verlag, Berlin, 2010.
[36] M. Menyhard, Mater. Sci. Forum 126 (1993) 205.
[37] Z. Erdélyi, Ch. Girardeaux, G.A. Langer, D.L. Beke, A. Rolland, J. Bernardini, J. Appl. Phys. 89 (2001) 3971.
[38] S.V. Divinski, M. Lohmann, Acta Mater. 49 (2001) 249.
[39] S.V. Divinski, C. Herzig, J. Mater. Sci. 43 (2008) 3900.
[40] S.V. Divinski, M. Lohmann, Sci. 11 (2003) 21.
[41] H. Edelhoff, S.V. Divinski, S. Prokofjev, Scripta Mater. 64 (2011) 374.
[42] A. Kwiatkowski da Silva, G. Leyson, M. Kuzmina, D. Ponge, M. Herbig, S. Sandlöbes, B. Gault, J. Neugebauer, D. Raabe, Acta Mater. 124 (2017) 305.
[43] S.J. Dillon, K. Tai, S. Chen, Curr. Opin. Solid State Mater. Sci. 20 (2016) 324.
[44] M. Kuzmina, M. Herbig, D. Ponge, S. Sandlöbes, D. Raabe, Science 349 (2015) 1080.
[45] D. Raabe, M. Herbig, S. Sandloebes, Y. Li, D. Tytko, M. Kuzmina, D. Ponge, P.P. Choi, Curr. Opin. Solid State Mater. Sci. 18 (2014) 253.
[46] B.B. Straumal, B.S. Bokstein, A.B. Straumal, A.L. Petelin, JETP Lett. 88 (2008) 537.
[47] X. Sauvage, G. Wilde, S.V. Divinski, Z. Horita, R.Z. Valiev, Mater. Sci. Eng. A 540 (2012) 1.
[48] B.B. Straumal, O.A. Kogtenkova, F. Muktepavela, K.I. Kolesnikova, M.F. Bulatov, P.B. Straumal, B. Baretzky, Mater. Lett. 159 (2015) 432.
[49] T. Frolov, Y. Mishin, Phys. Rev. B 85 (2012) 224107.
[50] J.M. Rickman, H.M. Chan, M.P. Harmer, J. Luo, Surf. Sci. 618 (2013) 88.
[51] A. Kirchner, B. Kieback, Scripta Mater. 64 (2011) 406.
[52] M.M. Gong, F. Liu, Y.Z. Chen, J. Alloys Comp. 682 (2016) 89.
[53] M. Menyhard, M. Yan, V. Vitek, Mater 42 (1994) 2783.
[54] S. Kiyohara, T. Mizoguchi, AIP Conf. Proc. 1763 (2016), 040001.
[55] T. Frolov, M. Asta, Y. Mishin, Phys. Rev. B 92 (2015), 020103.
[56] T. Frolov, S.V. Divinski, M. Asta, Y. Mishin, Phys. Rev. Lett. 110 (2013) 255502.
[57] J. Creuze, F. Berthier, R. Tetot, B. Legrand, Phys. Rev. B 62 (2000) 2813.
[58] J. Creuze, F. Berthier, R. Tetot, B. Legrand, Phys. Rev. Lett. 86 (2001) 5735.
[59] A.Y. Lozovoi, A.T. Paxton, M.W. Finnis, Phys. Rev. B 74 (2006) 155416.
[60] B.B. Straumal, A.R. Kilmametov, Yu. Ivanisenko, A.A. Mazilkin, O.A. Kogtenkova, L. Kurmanaeva, A. Korneva, P. Zięba, B. Baretzky, Int. J. Mater. Res. 106 (2015) 657.
[61] B. Straumal, A. Korneva, P. Zięba, Arch. Civil Mech. Eng. 14 (2014) 242.
[62] L.-S. Chang, E. Rabkin, B. Straumal, P. Lejcek, S. Hofmann, W. Gust, Scripta mater. 37 (1997) 729.
[63] B.B. Straumal, S.V. Dobatkin, A.O. Rodin, S.G. Protasova, A.A. Mazilkin, D. Goll, B. Baretzky, Adv. Eng. Mater. 13 (2011) 463.
[64] B.B. Straumal, A.O. Rodin, A.E. Shotanov, A.B. Straumal, O.A. Kogtenkova, B. Baretzky, Forum 333 (2013) 175.